Modeling of Torsional Compliance and Hysteresis Behaviors in Harmonic Drives

Hongwei Zhang, Saleh Ahmad, and Guangjun Liu, *Senior Member, IEEE*

***Abstract*—Nonlinear torsional compliance and hysteresis are associated with harmonic drives, and their accurate modeling is crucial for improving performance of the control system of harmonic drive-based devices such as robot joints. In this paper, a new approach is taken to model the torsional compliance and hysteresis behavior in harmonic drives. The proposed model is derived by modeling the compliance behavior of the flexspline and the wave generator instead of modeling the individual behaviors of the overall harmonic drive transmission. The hysteresis loss is captured by taking the wave generator torsional compliance into account. The proposed model is validated through numerical simulations and subsequently with experimental data.**

***Index Terms*—Compliance, harmonic drive, hysteresis, modeling, robot joint.**

I. Introduction

HARMONIC drives, invented in 1950s [1], are widely used in servo systems, such as robots, due to their desirable characteristics of near-zero backlash, compactness, light weight, high torque capacity, high gear ratio, and coaxial assembly. In the meantime, a number of attempts have been made toward the analytical modeling of harmonic drives. Volkov and Zubkov pioneered the investigation of harmonic drive transmission dynamics incorporating stiffness [2]. During the mid/late-1980s, Good *et al.* [3] and Kojima *et al.* [4] investigated the effects of the harmonic drive on robotic systems dynamic control. In [3], empirical data were used to show that performance degradation occurs if the joint flexibility is ignored in controller design of robot manipulators. The effect of nonlinear friction of harmonic drive transmissions on robotic systems performance was studied in [4]. Marilier and Richard [5] modeled the harmonic drive behavior including factors like nonlinear stiffness, soft-windup, and nonlinear friction torque. Later on, Hidaka *et al.* [6] reported the effects of transmission compliance and kinematic error on vibration during operation. In the existing literature, it has been a common observation that the aggregated effects of compliance, hysteresis loss, and kinematic error take part in the dynamics of harmonic drive transmission systems [7]. However, accurate modeling of the harmonic drive transmission system remains a challenging task. The hysteresis models proposed in [8], [9], and [10] require the derivative of torsional angle which is impractical to obtain because of measurement noise. Models of hysteresis behaviors of harmonic drives were also reported in [7], [11]–[13] where the coulomb friction effect is considered to be the source of hysteresis. In those models, only the sign of the derivative of the torsional angle is required. Dhaouadi *et al.* [14] used differential equations for modeling the hysteresis behavior in harmonic drives. In [15], Preisach model of hysteresis was used to capture the harmonic drive hysteretic behavior. Preisach model is also used to capture hysteretic behaviors of other physical systems such as piezoactuators [16]. Tjahjowidodo *et al.* [13] described the dynamics of harmonic drives using nonlinear stiffness characteristics combined with distributed Maxwell-slip elements that capture the hysteresis behavior. Curt *et al.* recently provided a more comprehensive hysteresis model [17].

In previous works, harmonic drive models are formulated by modeling each of its individual behaviors and then incorporating these models into equations governing the harmonic drive transmission. The downside of such an approach is the complexity of model(s), which stems from the complexity of behaviors, with nonlinear torsional compliance and hysteresis being on top of the list.

In this paper, the proposed model is derived by modeling the compliance behavior of the flexspline and the wave generator instead of modeling the individual behaviors of the overall harmonic drive transmission. Subsequently, the resulting model can capture the harmonic drive compliance and hysteresis loss behaviors by estimating the torque on the wave generator from motor output or estimating the torque on the wave generator from Maxwell-slip hysteresis model of friction. This study offers a simple model that can capture the hysteresis behavior present in harmonic drives. The model simplicity and adequate accuracy make it well suited for real-time applications.

A test setup has been built and used to experimentally evaluate the proposed harmonic drive model. The validity of the proposed model is confirmed by the agreement of its predicted torsional compliance with independent experimental data that were not used for model parameterization.

This paper is organized into six sections as follows. The harmonic drive mechanism is described in Section II, the proposed harmonic drive model is presented in Section III, parameter estimation is described in Section IV, experimental results are discussed in Section V, and concluding remarks are given in Section VI.

Manuscript received January 20, 2013; revised June 18, 2013, October 23, 2013, and January 29, 2014; accepted February 14, 2014. Date of publication April 1, 2014; date of current version October 3, 2014. Recommended by Technical Editor E. Richer. This work was supported in part by a research grant from the Natural Sciences and Engineering Research Council (NSERC) and in part by the Canada Research Chair (CRC) program.

The authors are with the Department of Aerospace Engineering, Ryerson University, Toronto, ON M5B 2K3, Canada (e-mail: hongwei.zhang@ryerson.ca; saleh1.ahmad@ryerson.ca; gjliu@ryerson.ca).

Color versions of one or more of the figures in this paper are available online at http://ieeexplore.ieee.org.

Digital Object Identifier 10.1109/TMECH.2014.2311382

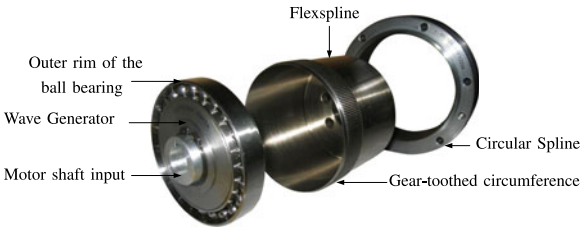

Fig. 1. Exploded view of a harmonic drive showing the three components.

II. Mechanism of Harmonic Drive

Harmonic drives consist of three main components as shown in Fig. 1. The wave generator is connected to a motor, the circular spline is connected to the joint base, and the flexspline is sandwiched in between the circular spline and the wave generator and connected to the joint output. The wave generator consists of an elliptical disk, called wave generator plug, and an outer raced ball-bearing assembly. The wave generator plug is inserted into the ball-bearing assembly, thereby giving the bearing an elliptical shape as well. The flexspline is a thin cylindrical cup with external teeth at the open end of the cup having a slightly smaller pitch diameter than the internal teeth of the circular spline. Once assembled, the flexspline fits tightly over the wave generator, therefore, when the wave generator plug is rotated the flexspline deforms and molds into the shape of the rotating ellipse. The circular spline has two more teeth than the flexspline, because of which there exists a small phase difference between the corresponding teeth in engagement. This phase difference makes the sliding effect unavoidable which in turn causes energy losses and raises the temperature up to the equilibrium point that is around 60–70 °C [8]. Clearly, any deviation of the teeth from an ideal shape results in a torque-transmission ripple, as well as the well-known errors in gear ratio that is named the kinematic error. Another major source of gear error and torque-transmission ripple is out of roundness of the circular spline [18].

III. Harmonic Drive Model

A. Basic Model

The kinematic relationship, as explained in [19], equates the angular positions at the three components of the harmonic drive and is given by

$$\theta_w = (N+1)\,\theta_c - N\theta_F \tag{1}$$

$$\omega_w = (N+1)\,\omega_c - N\omega_F \tag{2}$$

where N denotes the gear ratio, θ_w, θ_c, and θ_F refer to the angular position of wave generator, circular spline, and flexspline, respectively, and ω_w, ω_c, and ω_F denote the corresponding angular velocities. The static force balance between the elements can be described by the following equation as in [17]

$$T_w = \frac{1}{N+1}T_c = -\frac{1}{N}T_F \tag{3}$$

where T_w, T_c, T_F represent the torque at the wave generator, circular spline, and flexspline, respectively. To be consistent with the existing literature and general existing applications, where the circular spline is usually fixed leaving the wave generator and flexspline for input and output, so that $\theta_c = \omega_c = 0$, and the reaction torque T_c is not of a concern. Therefore, (1) to (3) can be simplified as

$$\theta_w = -N\theta_F \tag{4}$$

$$\omega_w = -N\omega_F \tag{5}$$

$$T_w = -\frac{1}{N}T_F. \tag{6}$$

The above equations represent the harmonic drive's ideal linear input/output relationship, and the harmonic drive transmission is treated as a perfectly rigid gear reduction mechanism. The empirical measurements of the input/output relationship provided in the cited literature clearly show that the output is not linearly related to the input [17]. The causes of this nonlinearity are compliance in the harmonic drive components, nonlinear friction forces, and the kinematic error due to gear meshing [20], [21], which takes a more comprehensive harmonic drive model to incorporate.

B. Basic Model With Compliance and Friction

The compliance of flexspline and harmonic drive friction is considered in this section. Other aspects of the harmonic drive behavior such as hysteresis loss, wave generator compliance, and nonlinearity are left for later consideration. When harmonic drive friction is considered, the basic compliance model can be described by (7)–(9)

$$\theta_w = -N\theta_{Fi} \tag{7}$$

$$\omega_w = -N\omega_{Fi} \tag{8}$$

$$T_w = -\frac{1}{N}(T_F - T_{Fr}) \tag{9}$$

where T_{Fr} is the friction torque, θ_{Fi} and ω_{Fi} denote the angular position and angular velocity at the flexspline gear-side (gear-toothed circumference), respectively. As described in a manufacturer's catalog [19], the stiffness curve features increasing stiffness with displacement and hysteresis loss behavior. To represent the nonlinear stiffness, the manufacturer suggests using piecewise linear approximations [19], while several researchers have used a cubic polynomial approximation [2], [6]. The nonlinear flexspline output torque T_F is approximated by a third-order polynomial function of the torsional angle as

$$T_F = a_1 \triangle\theta + a_3(\triangle\theta)^3 \tag{10}$$

where $\triangle\theta$ is the torsional angle of the harmonic drive, a_1 and a_3 are constants to be determined.

Another method of estimating the torsional angle is described in [19], where $\triangle\theta$ is approximated by a piecewise linear function of the output torque as shown in Fig. 2(b). The piecewise linear

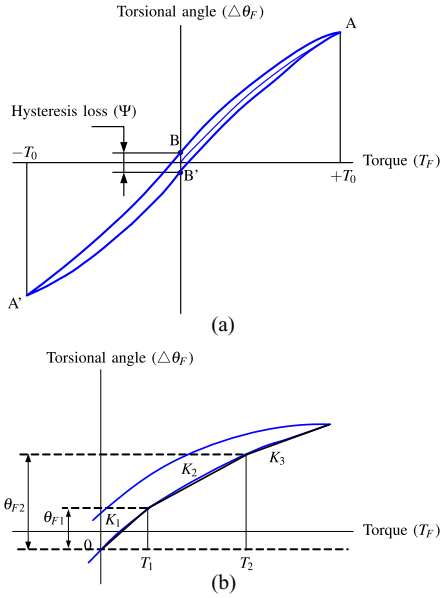

Fig. 2. Typical stiffness and hysteresis curve of a harmonic drive. (a) Stiffness and hysteresis curve. (b) Straight lines approximation.

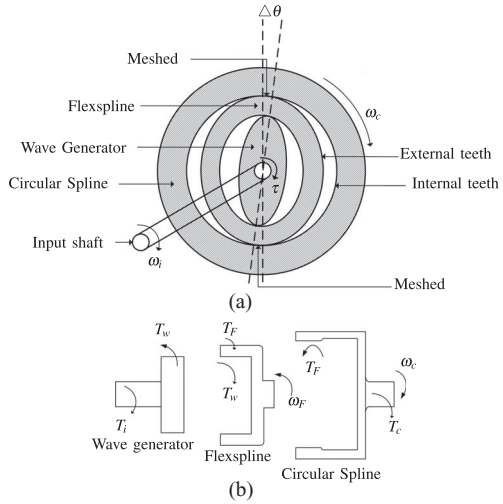

Fig. 3. (a) Wave generator axes displacement. (b) Free body diagrams.

function is given by

$$\triangle\theta = \begin{cases} \dfrac{T_F}{K_1}, & T_F \le T_1 \\ \dfrac{T_1}{K_1} + \dfrac{T_F - T_1}{K_2}, & T_1 < T_F < T_2 \\ \dfrac{T_1}{K_1} + \dfrac{T_2 - T_1}{K_2} + \dfrac{T_F - T_2}{K_3}, & T_F \ge T_2 \end{cases} \tag{11}$$

where K_1, K_2, K_3, T_1, and T_2 are given by the manufacturer.

When the harmonic drive torsion is assumed to be caused by flexspline only, the torsional angle can also be determined as

$$\triangle\theta = \theta_{Fo} - \theta_{Fi} \tag{12}$$

where θ_{Fo} denotes the flexspline angular position at the load side which is measured using the link-side encoder. In general, only the wave generator input position (motor's angle) and flexible output position (joint's angle) are measurable. These available position measurements can be used to calculate the torsional angle of the harmonic drive using the following relation:

$$\triangle\theta = \theta_{Fo} + \frac{\theta_w}{N}. \tag{13}$$

The model described in this section does not incorporate the hysteresis loss, which is a phenomenon that is more difficult to model than the stiffness, and consequently, it is often ignored. It is well known that hysteresis influences the position accuracy of harmonic drive transmissions [17]. A suitable harmonic drive model is essential for high performance robot joint control, as required by our previous work on modular robot control. Hysteresis behavior of harmonic drives is usually modeled using phenomenological-based hysteresis models, like the Preisach or Prandtl–Ishlinskii model that is based on parallel connection of stop-type operators. This results in a complex harmonic drive model with a large number of parameters that need to be estimated. The objective of this paper is to derive a simple control-oriented model that can capture the nonlinear torsional compliance and hysteresis behaviors of harmonic drives.

C. Proposed Harmonic Drive Model

Not many researchers have investigated the main sources of flexibility in harmonic drive transmissions. One was the team of Margulis and Volkov [22] who reported the results of experiments they performed on harmonic drives having two-cam wave generators. They conclude that the deformation of wave generator was the main contributor in total torsional compliance. They also noticed that high radial forces on the wave generator can cause substantial radial deflection allowing relative rotation across transmission. A similar observation was made by Shigeo *et al.* [23] who performed similar stiffness tests on conventional harmonic drives with elliptical bearing wave generators. They observed that the deflection in wave generator bearing, caused by high radial forces exerted on the wave generator, can significantly influence transmission torsion. To adequately model the harmonic drive behavior, the flexibility of both the flexspline and the wave generator must be considered. It will be shown that a high fidelity harmonic drive model able to capture the hysteresis loss is achieved by modeling the compliance of the wave generator in addition to the compliance of the flexspline. As explained about the harmonic drive mechanism in Section II, when the wave generator's rigid elliptical inner-race is rotated, the flexspline molds into the rotating elliptical shape but does not rotate with it. The axes of these two elliptical shapes (Wave generator inner-race and flexspline) are not always aligned, as depicted in Fig. 3. The reason behind this misalignment is the compliance of the wave generator, namely, the ball bearing [23]. This misalignment is dependent on the magnitude of the torque applied to the wave generator plug as well as the load torque. This compliance of the wave generator needs to be taken into account when modeling the harmonic drive compliance. In this section, a model of the compliance of the flexspline and the wave generator is derived first, and then the complete compliance model of the harmonic drive is given.

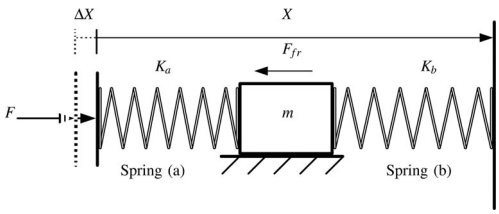

Fig. 4. Two springs system. K_a, K_b represent spring (a) and (b) constant, respectively; ΔX is the total displacement; F_{fr} is the friction torque; F_a and F_b are the spring forces.

Remark 1: The compliance of wave generator can be readily understood by observing the curve shown in Fig. 2(a). The torsional angle could have a value between B and B' at zero flexspline torque, which clearly indicates that this torsion is not due to flexspline flexibility. This deformation is due to the torque at the wave generator and cannot reach zero because of the hysteresis.

The following assumption is made for deriving the model for the harmonic drive.

Assumption 1: The angle at the flexspline input (gear-toothed circumference) is assumed to be equal to the angle of the wave generator output (outer rim of the ball bearing).

This assumption always holds when there is no relative motion between the wave generator and the flexspline, which is usually guaranteed by the mechanical structure of the harmonic drive.

Let the flexspline and wave generator torsion be defined as

$$\triangle\theta_F = \theta_{Fo} - \theta_{Fi} \tag{14}$$

$$\triangle\theta_w = \theta_{wo} - \theta_{wi} \tag{15}$$

where θ_{wo}, θ_{wi} denote the positions of the wave generator outside part (ball bearing outer rim) and the center part (wave generator plug), respectively. θ_{Fi} and θ_{Fo} have the same implications as those in (7) and (12), respectively.

The flexspline and wave generator torque can be modeled as

$$T_F = K_F \triangle\theta_F \tag{16}$$

$$T_w = K_w \triangle\theta_w \tag{17}$$

where K_F and K_w denote the stiffness of flexspline and wave generator, respectively.

In order to model the harmonic drive compliance, consider its mechanical system analogy: the spring-mass system with two springs and a mass shown in Fig. 4. The behavior of the harmonic drive rotational compliance can be described by the behavior of this serial spring-mass system. As an illustration of this fact, assume that spring (a) represents the wave generator compliance, spring (b) represents the flexspline compliance, mass (m) is the serial analogy of the harmonic drive inertia which is composed of the wave generator and flexspline, and F_{fr} is the harmonic drive friction. When F increases from zero, spring (a) is compressed and spring (b) stays at its initial position as long as $F < F_{fr}$. When $F > F_{fr}$, spring (b) is compressed by $(F - F_{fr})$, and the displacement ΔX can be described by $\triangle X = F_a/K_a + F_b/K_b$. Moreover, spring-mass systems exhibit friction-induced hysteresis behavior which is similar to that observed in harmonic drives [24]–[27]. Therefore, the two-spring system describes the stiffness and hysteresis behavior of the harmonic drive transmission. To study the analogy of this system to the harmonic drive, simulations were used to compare the typical stiffness curve of the harmonic drive, shown in Fig. 2(a), to that of the two-spring system. Fig. 5 shows the force of spring (b) F_b versus the force applied to spring (a) F_a; and Fig. 6 shows the stiffness curve and the hysteresis loss caused by friction for the harmonic drive and the two-spring system. From Fig. 6, it is clear that the two-spring system stiffness curve replicates the shape of harmonic drive typical stiffness and hysteresis curve. The mismatch between these two shapes stems from the fact that the spring's stiffness is assumed linear whereas the harmonic drive stiffness is nonlinear.

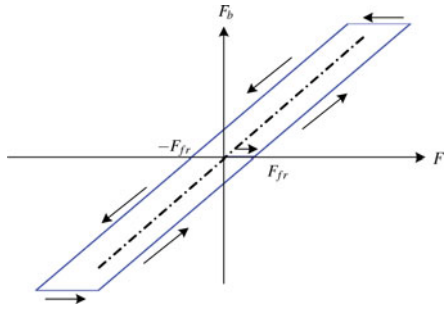

Fig. 5. Spring (b) force versus force applied to spring (a).

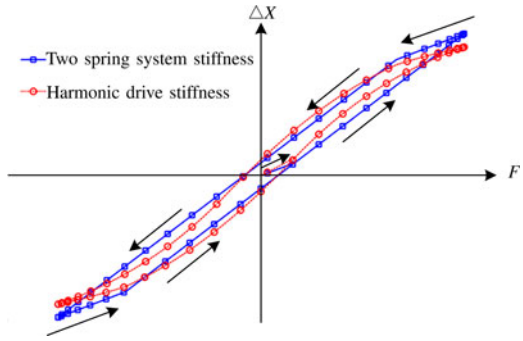

Fig. 6. Stiffness curve of the mass-spring system and that of harmonic drives.

When considering the compliance of wave generator, (7) becomes

$$\theta_{wo} = -N\theta_{Fi}. \tag{18}$$

It should be noted that θ_{Fi} cannot be measured. The harmonic drive torsion can be obtained by using the following expression:

$$\triangle\theta = \theta_{Fo} + \frac{\theta_{wi}}{N}. \tag{19}$$

By adding and subtracting the terms θ_{Fi} and $\frac{\theta_{wo}}{N}$ to (19), one obtains

$$\triangle\theta = \theta_{Fo} - \theta_{Fi} + \left(\theta_{Fi} + \frac{\theta_{wo}}{N}\right) - \left(\frac{\theta_{wo}}{N} - \frac{\theta_{wi}}{N}\right). \tag{20}$$

Based on the assumption that there is no relative motion between the wave generator output and the flexspline input, we have $\theta_{wo} + N\theta_{Fi} = 0$. Substituting (14) and (15) into (20) yields

$$\triangle\theta = \triangle\theta_F - \triangle\theta_w/N. \tag{21}$$

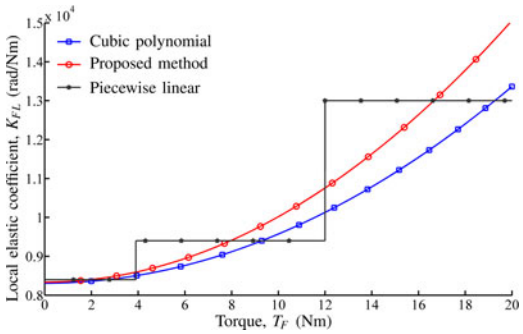

Fig. 7. Simulation results of local elastic coefficient.

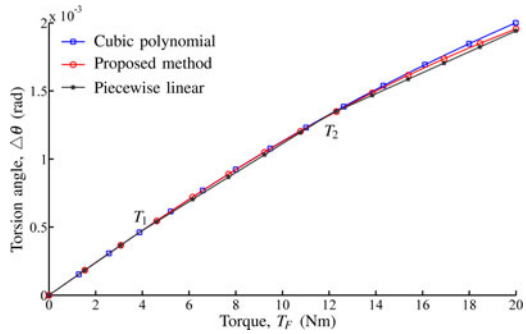

Fig. 8. Stiffness curves for piecewise linear model, cubic polynomial model, and proposed model.

Equations (10) and (11) describe the nonlinear compliance of the flexspline, but are inconvenient to use in control system design. Equation (11) has discontinuity and is not accurate as the curve was approximated by three straight lines. Equation (10) does not have discontinuity, but not convenient to use as the inverse is required. It is more suitable to describe the torsional angle as a function of the torque, especially for control purposes. By observing (10) and the stiffness curve in Fig. 2(a), it is clear that the local elastic coefficient increases as T_F increases. Let us define, the local elastic coefficient K_{FL} as

$$K_{FL} = \frac{dT_F}{d\triangle\theta_F}.$$

Considering the symmetric property of the harmonic drive stiffness and using Taylor expansion, the local elastic coefficient can be approximated by

$$K_{FL} = K_{F0}\left(1 + (C_F T_F)^2\right) \tag{22}$$

where K_{F0} and C_F are constants to be determined. If $K_{F0} \neq 0$, then the flexspline torsion can be calculated as

$$\triangle\theta_F = \int_0^{T_F} \frac{dT_F}{K_{FL}}. \tag{23}$$

By substituting the expression for K_{FL} in (22) into (23), one can obtain the following expression:

$$\triangle\theta_F = \frac{\arctan(C_F T_F)}{C_F K_{F0}} \tag{24}$$

where arctan(.) is the arctangent function.

The derived model has been compared with the linear piecewise model and the cubic polynomial model through simulations. Figs. 7 and 8 show the simulation results for piecewise linear model, cubic polynomial model, and proposed model. The results show that the proposed stiffness model matches others. At zero torque output, the harmonic drive torsional deformation can range from $-\Psi/2$ to $\Psi/2$ where Ψ is the hysteresis loss. At rated torque, this deformation range drops down to zero sharply which implies that the stiffness of wave generator increases sharply. In order to replicate the hysteresis shape of this stiffness curve, the local elastic coefficient of wave generator can be modeled as

$$K_{wL} = K_{w0} e^{C_w |T_w|} \tag{25}$$

where K_{w0} and C_w are constants to be determined. If $K_{w0} \neq 0$, then the wave generator torsional angle can be calculated using the following relation:

$$\triangle\theta_w = \int_0^{T_w} \frac{dT_w}{K_{wL}}. \tag{26}$$

Substituting (25) into (26) yields

$$\triangle\theta_w = \frac{\text{sign}\,(T_w)}{C_w K_{w0}}\left(1 - e^{-C_w |T_w|}\right). \tag{27}$$

Finally, the total deformation of the harmonic drive is obtained by substituting the flexspline and wave generator deformation given in (24) and (27) into (21)

$$\triangle\theta = \frac{\arctan(C_F T_F)}{C_F K_{F0}} - \frac{\text{sign}\,(T_w)}{C_w N K_{w0}}(1 - e^{-C_w |T_w|}). \tag{28}$$

Remark 2: Information about motion-reversal points is implicit in (28) due to the fact that T_w incorporates information about the direction-dependent friction torque.

IV. Parameter Estimation

In this section, a systematic way of estimating the parameters of the proposed harmonic drive model is described. The typical stiffness and hysteresis curve of the harmonic drive, as provided by manufacturer's specification sheet [19], is depicted in Fig. 2. From the stiffness and hysteresis curve shown in Fig. 2(b), the local elastic coefficients at torque $T_1/2$ and $(T_1 + T_2)/2$ are K_1 and K_2, respectively. These local elastic coefficients can be calculated using (22), as follows:

$$K_1 = K_{F0}\left(1 + (C_F T_1/2)^2\right) \tag{29}$$

$$K_2 = K_{F0}(1 + (C_F(T_1 + T_2)/2)^2). \tag{30}$$

By solving (29) and (30) for K_{F0} and C_F, one can obtain the following:

$$K_{F0} = K_1 + \frac{(K_1 - K_2)T_1^2}{(T_1 + T_2)^2 - T_1^2} \tag{31}$$

$$C_F = 2\sqrt{\frac{K_2 - K_1}{K_1(T_1 + T_2)^2 - K_2 T_1^2}}. \tag{32}$$

From the typical stiffness and hysteresis curve shown in Fig. 2(b), the stiffness of the wave generator at zero output torque can be estimated using the following relation:

$$K_{w0} = \frac{2T_{fs}}{N\Psi} \tag{33}$$

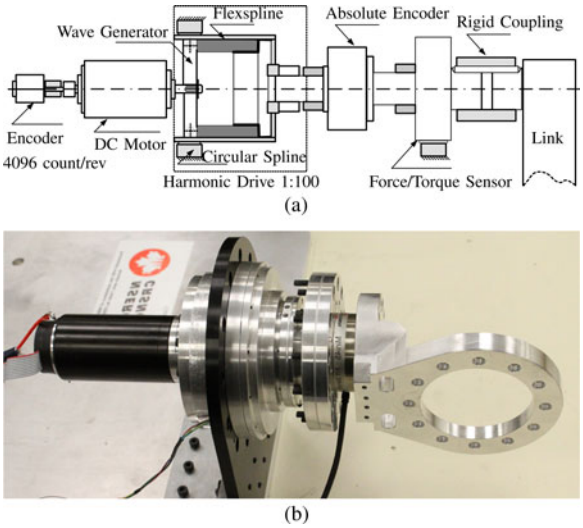

Fig. 9. Experimental setup. (a) Schematic diagram and (b) Picture of the experimental test apparatus.

where Ψ denotes the hysteresis loss and T_{fs} is the harmonic drive's starting torque. From (27), the maximum torsion of the wave generator at one direction is $1/(C_w N K_{w0})$. It is also evident from Fig. 2 that the total deformation due to the wave generator compliance at one direction is half of the hysteresis loss Ψ. Therefore, one can write

$$0.5\Psi = \frac{1}{C_w N K_{w0}}. \tag{34}$$

Solving (34), one can obtain

$$C_w = \frac{2}{N K_{w0} \Psi}. \tag{35}$$

V. Experimental Results

To investigate the behavior of harmonic drive systems, a test station is set up as shown in Fig. 9. In this experimental setup, the harmonic drive is driven by a brushed DC motor from Maxon, model 218014. Its weight is 480 g, with maximum rated torque of 188 mNm, and torque constant of 0.321 Nm/amp. A linear power amplifier and the Q8 data acquisition board from Quanser, Inc., are used to drive the motor and collect experimental data. The harmonic drive in the setup is SHD-17-100-2SH with gear ratio of 100:1, and rated torque of 16 Nm from Harmonic Drive AG. The link-side position is measured using Netzer absolute position electric encoder with 19-bit resolution and the link-side torque is measured using ATI six-axis force/torque sensor. The motor-side position is measured with 4096 count/rev incremental encoder from Maxon motor, part number is 225 787. Two experiments are presented in the following. In the first experiment, a controlled torque was applied to the wave generator with the output link fixed (output rotationally locked). The harmonic drive torsional angle was measured using two encoders, one on the motor-side and another on the link-side. The output torque was measured by link-side force sensor, and applied torque at wave generator is calculated from the commanded torque. In the second experiment, a position controller was used to hold the wave generator at a fixed position (input rotationally locked),

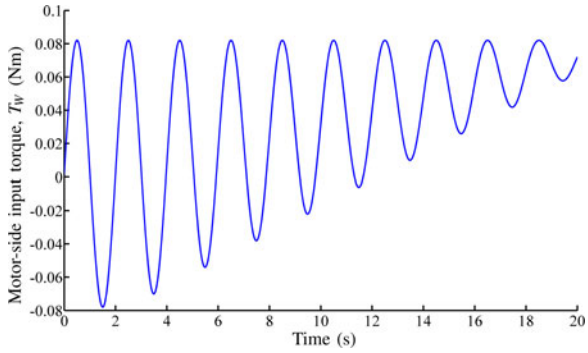

Fig. 10. Motor-side input torque signal history.

and both forward and backward torque are applied to the link. The link-side torque was measured by link-side force sensor, and the wave generator torque was calculated using static friction model. From manufacturer's literature [19], the following parameters are obtained:

$$K_1 = 8.4 \times 10^3 \text{ Nm/rad}, \quad K_2 = 9.4 \times 10^3 \text{ Nm/rad}$$
$$T_1 = 3.9 \text{ Nm}, \quad T_2 = 12 \text{ Nm}.$$

K_{F0} and C_F can be obtained by solving (31) and (32) and the results are given by

$$K_{F0} = 8.333 \times 10^3 \text{ Nm/rad}$$
$$C_F = 0.089 \text{ (Nm)}^{-1}.$$

The hysteresis loss at zero output torque Ψ can be easily obtained from the experiential results shown in Fig. 14

$$\Psi = 1.8 \times 10^{-4} \text{ rad}.$$

Both the starting torque T_{fs} used for estimating K_{w0}, and the back-driving torque T_{fb} used for estimating the wave generator torque in the later experiment, are determined experimentally. T_{fs} is determined by gradually increasing the joint torque command from zero while simultaneously monitoring the motor-side incremental encoder readings. The starting torque T_{fs} is equal to the motor torque at the first pulse of the motor-side incremental encoder. The back-driving torque T_{fb} was determined by applying torque to the link-side port. T_{fb} is equal to the torque sensor measurement at the first pulse of the motor-side incremental encoder

$$T_{fs} = 0.012 \quad \text{Nm} \quad T_{fb} = 2.0 \text{ Nm}.$$

K_{w0} can be calculated by plugging T_{fs} and Ψ into (33)

$$K_{w0} = (2 \times 0.012)/(100 \times 1.8 \times 10^{-4}) = 1.33 \text{ Nm/rad}.$$

By plugging K_{w0} and Ψ into (35), one can obtain

$$C_w = (2)/(100 \times 1.33 \times 1.8 \times 10^{-4}) = 83.5 \text{ (Nm)}^{-1}.$$

These parameters are calculated to be used with the harmonic drive model of (27). Once the model parameters are calculated and/or estimated, the model is tested by comparing model predicted results with the experimental data. In the first experiment, to observe the harmonic drive stiffness and hysteresis behavior, a monotonically decreasing torque command signal is used to drive the DC motor as depicted in Fig. 10. The harmonic drive

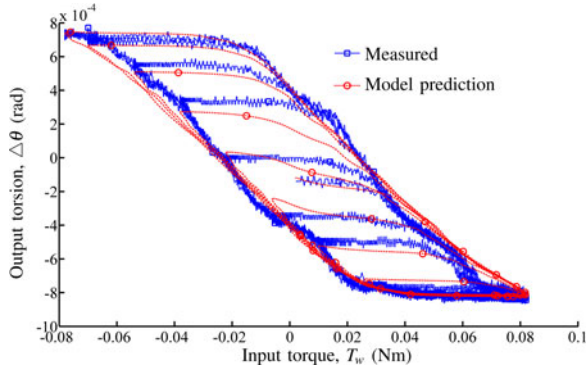

Fig. 11. Motor-side input torque versus output torsion.

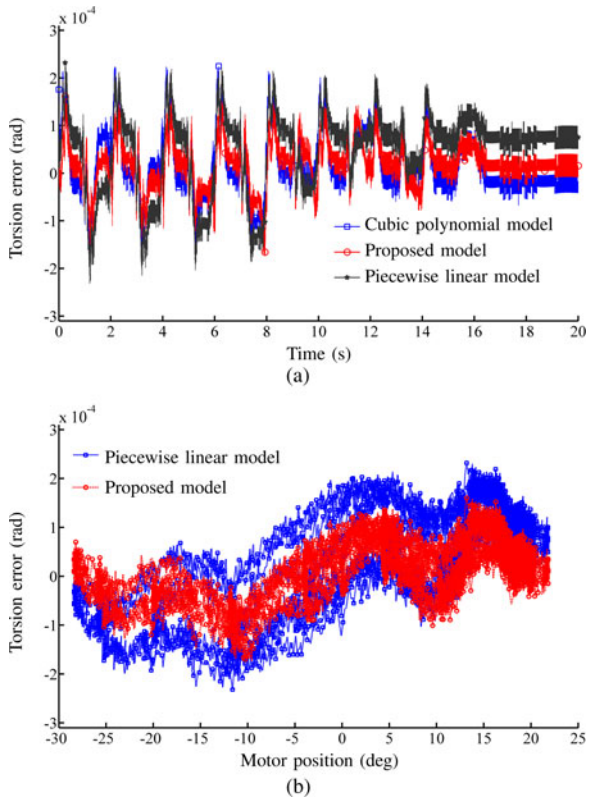

Fig. 12. Estimation error comparison. (a) Estimation error versus time. (b) Estimation error versus motor positions.

torsional angle is measured simultaneously using the encoders mounted on the motor-side and the output-side. The empirical data collected from the first experiment along with the model predicted torsion versus the input torque values are depicted in Fig. 11. The estimation error of the cubic polynomial model given in (10), the piecewise linear compliance model given in (11), and that of the proposed model in (28) are shown in Fig. 12(a). The results show that the proposed model can achieve better torsion estimation. This is due to the fact that the proposed model captures the hysteresis behavior of the harmonic drive. As shown in Fig. 12(b), when comparing the proposed model to the piecewise linear model, the estimation errors form two similar curves. The pattern of the two similar curves represents the kinematic error, while the distance between the two curves

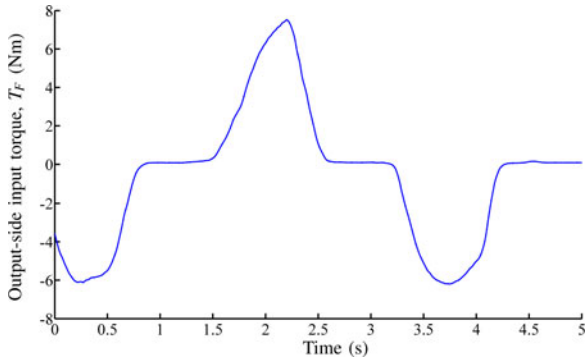

Fig. 13. External torque applied on the output-side.

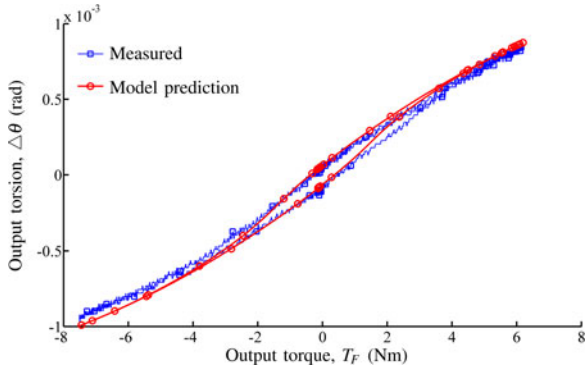

Fig. 14. Output torque versus output torsion.

is hysteresis error. The proposed model reduces the distance between the two curves, that is, reduces the hysteresis error. Based on this experiment, the rms value of estimation errors was reduced from 9.5×10^{-5} rad to 4.9×10^{-5} rad; the maximal estimation error was also reduced from $\pm 2.3 \times 10^{-4}$ to $\pm 1.7 \times 10^{-4}$ rad. The remaining error is caused by the unmodeled kinematic error. The simple and efficient compliance and hysteresis model proposed in this paper achieves estimation errors similar to those achieved by more complex models, e.g., the work presented in [17]. In the second experiment, a bidirectional external torque is applied on flexspline side as shown in Fig. 13. The wave generator torque is estimated using the following equations where the measured back-driving friction torque T_{fb} was used:

$$\begin{aligned} &\text{If } T_F(t) + NT_w(t-1) > T_{fb}, && T_w(t) = -(T_F(t) - T_{fb})/N \\ &\text{if } T_F(t) - NT_w(t-1) > -T_{fb}, && T_w(t) = -(T_F(t) + T_{fb})/N \\ &\text{else}, && T_w(t) = T_w(t-1). \end{aligned} \tag{36}$$

The harmonic drive torsional angle is obtained by substituting the measured link-side position and the motor-side position into (13). Comparison between the measured torsional angle with the torsion estimated using (28) is shown in Fig. 14. The agreement between the predicted torsional compliance and the experimental data in both experiments confirmed the validity of the proposed model.

VI. Conclusion

A novel compliance model of harmonic drives has been presented. The proposed model captures the nonlinear stiffness and hysteresis behavior of harmonic drive transmissions. A new approach to modeling the hysteresis behavior in harmonic drives is presented, in which the hysteresis loss is captured by taking the wave generator torsional compliance into account. The method of estimating the parameters of the proposed harmonic drive model is described in details. Experimental results have confirmed the simplicity and effectiveness of the proposed model. With its high efficiency and accuracy, the proposed model opens an avenue for future control designs of robot and other machines using harmonic drives. A thorough and rigorous comparison between the proposed model and those reported in the literature is also considered as future work.

References

[1] C. W. Musser. (1955). "Strain wave gearing," U.S. Patent 2 906 143 03 23, [Online]. Available:http://www.google.com/patents?vid=2906143

[2] D. P. Volkov and Y. Zubkov, "Vibrations in a drive with a harmonic gear transmission," *Russ. Eng. J.*, vol. 58, no. 5, pp. 11–15, 1978.

[3] M. C. Good, L. M. Sweet, and K. L. Strobel, "Dynamic models for control system design of integrated robot and drive systems," *J. Dyn. Syst., Meas., Control*, vol. 107, no. 1, pp. 53–59, 1985.

[4] H. Kojima, K. Taguti, and H. Tuji, "Robot vibrations caused by torque ripples in power transmission mechanisms," *Trans. Jpn. Soc. Mech. Eng. C*, vol. 55, no. 517, pp. 2390–2395, 1989.

[5] T. Marilier and J. A. Richard, "Non-linear mechanic and electric behavior of a robot axis with a 'harmonic-drive' gear," *Robot. CIM-INT Manuf.*, vol. 5, no. 2/3, pp. 129–136, 1989.

[6] T. Hidaka, T. Ishida, Y. Zhang, M. Sasahara, and Y. Tanioka, "Vibration of a strain-wave gearing in an industrial robot," in *Proc. Int. Power Transmiss. Gear. Conf.*, Chicago, IL, USA, May 1990, pp. 789–794.

[7] H. Schempf and D. R. Yoerger, "Study of dominant performance characteristics in robot transmissions," *J. Mech. Des.*, vol. 115, no. 3, pp. 472–482, 1993.

[8] N. M. Kircanski and A. A. Goldenberg, "An experimental study of nonlinear stiffness, hysteresis, and friction effects in robot joints with harmonic drives and torque sensors," *Int. J. Robot. Res.*, vol. 16, no. 2, pp. 214–239, 1997.

[9] W. Seyfferth, A. J. Maghzal, and J. Angeles, "Nonlinear modeling and parameter identification of harmonic drive robotic transmissions," in *Proc. IEEE Int. Conf. Robot. Autom.*, Nagoya, Japan, May 1995, pp. 3027–3032.

[10] H. D. Taghirad and P. R. Belnger, "Modeling and parameter identification of harmonic drive systems," *J. Dyn. Syst., Meas., Control*, vol. 120, no. 4, pp. 439–444, 1998.

[11] T. D. Tuttle and W. P. Seering, "A nonlinear model of a harmonic drive gear transmission," *IEEE Trans. Robot. Autom.*, vol. 12, no. 3, pp. 368–374, Jun. 1996.

[12] C. W. Kennedy and J. P. Desai, "Modeling and control of the Mitsubishi PA-10 robot arm harmonic drive system," *IEEE/ASME Trans. Mechatronics*, vol. 10, no. 3, pp. 263–274, Jun. 2005.

[13] T. Tjahjowidodo, F. Al-Bender, and H. V. Brussel, "Theoretical modelling and experimental identification of nonlinear torsional behaviour in harmonic drives," *Mechatronics*, vol. 23, no. 5, pp. 497–504, 2013.

[14] R. Dhaouadi, F. H. Ghorbel, and P. S. Gandhi, "A new dynamic model of hysteresis in harmonic drives," *IEEE Trans. Ind. Electron.*, vol. 50, no. 6, pp. 1165–1171, Dec. 2003.

[15] I. D. Mayergoyz, *Mathematical Models of Hysteresis and Their Applications* (Series in Electromagnetism). Boston, MA, USA: Elsevier, 2003.

[16] Y. L. Zhang, M. L. Han, M. Y. Yu, C. Y. Shee, and W. T. Ang, "Automatic hysteresis modeling of piezoelectric micromanipulator in vision-guided micromanipulation systems," *IEEE/ASME Trans. Mechatronics*, vol. 17, no. 3, pp. 547–553, Jun. 2012.

[17] P. Curt, R. J. Thomas, and S. Deming, "A high-fidelity harmonic drive model," *J. Dyn. Syst., Meas., Control*, vol. 134, no. 1, pp. 11002–11013, 2012.

[18] T. W. Nye and R. P. Kraml, "Harmonic drive gear error: Characterization and compensation for precision pointing and tracking," in *Proc. 25th Aerosp. Mech. Symp.*, 1991, pp. 237–252.

[19] *CSD and SHD Ultra-flat Component Sets and Gearheads*, Harmonic Drive Technologies, Tokyo, Japan 2012.

[20] F. Ghorbel, P. S. Gandhi, and F. Altpeter, "On the kinematic error in harmonic drive gears," *ASME J. Mech. Des.*, vol. 123, pp. 90–97, Mar. 2001.

[21] T. Tuttle, "Understanding and modeling the behavior of a harmonic drive gear transmission," MIT Artificial Intelligence Laboratory, Cambridge, MA, USA, Tech. Rep. 1365, 1992.

[22] M. V. Margulis and D. P. Volkov, "Calculation of the torsional rigidity of a harmonic power drive with a disc generator," *Soviet Eng. Res.*, vol. 7, no. 6, pp. 17–19, Jun. 1987.

[23] Y. Shigeo, S. Ishizuka, T. Yamaguchi, and I. Masaki, "Torsional stiffness of harmonic drive reducers," *Trans. Jpn. Soc. Mechanic. Eng. C,* (in Japanese), vol. 55, no. 509, pp. 216–221, Jan. 1989.

[24] F. Al-Bender, W. Symens, J. Swevers, and H. V. Brussel, "Theoretical analysis of the dynamic behavior of hysteresis elements in mechanical systems," *Int. J. Non-Lin. Mech.*, vol. 39, pp. 1721–1735, 2004.

[25] B. Drincic and D. Bernstein, "A multiplay model for rate-independent and rate-dependent hysteresis with nonlocal memory," in *Proc. 48th IEEE Conf. Decis. Control*, Shanghai, China, Dec. 2009, pp. 8381–8386.

[26] K. Padthe, B. Drincic, D. D. R. J. Oh, S. D. Fassois, and D. S. Bernstain, "Duhem modeling of friction-induced hysteresis," *IEEE Control Syst. Mag.*, vol. 28, no. 5, pp. 90–107, Oct. 2008.

[27] A. Padthe, J. Oh, and D. Bernstein, "On the Lugre model and friction-induced hysteresis," in *Proc. Amer. Control Conf.*, Minneapolis, MN, USA, Jun. 2006, pp. 3247–3252.

Hongwei Zhang received the B.Sc. degree from the University of Science and Technology of China, Hefei, China, in 1990, the M.E. degree from Tongji University, Shanghai, China, in 1993, and the Ph.D. degree, from Ryerson University, Toronto, ON, Canada, in 2013.

His research interests include multiple working modes control design for modular and reconfigurable robots. His research also focuses on the precise modeling of harmonic drive transmission taking into account the hysteresis properties, nonlinear friction dissipation, and the kinematic error.

Saleh Ahmad received the B.Sc. degree in electronics engineering from Sebha University, Sabha, Libya, in 1999, the M.Sc. degree in control engineering from Lakehead University, Thunder Bay, ON, Canada, in 2008, and the Ph.D. degree from Ryerson University, Toronto, ON, Canada, in 2013.

He is currently a Postdoctoral Fellow in the Department of Aerospace Engineering, Ryerson University. His current research interests include harmonic drive modeling, mobile manipulation, and multiple working modes control design for modular and reconfigurable robots.

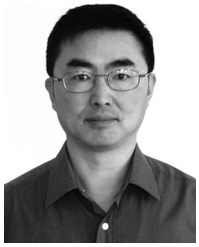

Guangjun Liu (M'99–SM'08) received the B.E. degree from the University of Science and Technology of China, Hefei, China, in 1984, the M.E. degree from the Chinese Academy of Sciences, Shenyang Institute of Automation, Shenyang, China, in 1987, and the Ph.D. degree from the University of Toronto, Toronto, ON, Canada, in 1996.

From 1997 to 1999, he was a Systems Engineer and a Design Lead for Honeywell Aerospace Canada, where he was engaged in the Boeing X-32 program. During 1996, he was a Postdoctoral Fellow at the Massachusetts Institute of Technology, Cambridge, MA, USA. He is currently a Professor and Canada Research Chair in control systems and robotics in the Department of Aerospace Engineering, Ryerson University, Toronto, ON, Canada. He has authored or coauthored more than 160 papers in international journals and conference proceedings. His current research interests include control systems and robotics, particularly in modular and reconfigurable robots, mobile manipulators, and aircraft systems.

Dr. Liu is a Technical Editor of the IEEE/ASME Transactions on Mechatronics and a Licensed Member of the Professional Engineers of Ontario, Canada.